Expert Systems With Applications 238 (2024) 122129

Contents lists available at ScienceDirect

Expert Systems With Applications

journal homepage: www.elsevier.com/locate/eswa

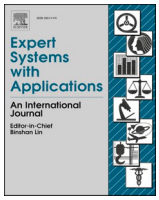

Incremental learning-based cascaded model for detection and localization of tuberculosis from chest x-ray images

Satvik Vats [a], Vikrant Sharma [a], Karan Singh [b], Anvesha Katti [c,j,*], Mazeyanti Mohd Ariffin [c], Mohammad Nazir Ahmad [d], Ali Ahmadian [e,f,g,*], Soheil Salahshour [f,h,i,*]

[a] Computer Science & Engineering, Graphic Era Hill University, Dehradun, Uttarakhand, India
[b] School of Computer and Systems Sciences, Jawaharlal Nehru University, New Delhi, 110067, India
[c] Positive Computing Research Cluster, Universiti Teknologi Petronas, 32610 Seri Iskandar, Malaysia
[d] Institute of Visual Informatics, Universiti Kebangsaan Malaysia (UKM), Bangi 43600 Selangor, Malaysia
[e] Decisions Lab, Mediterranea University of Reggio Calabria, Reggio Calabria, Italy
[f] Faculty of Engineering and Natural Sciences, Istanbul Okan University, Istanbul, Turkey
[g] Department of Computer Science and Mathematics, Lebanese American University, Beirut, Lebanon
[h] Faculty of Engineering and Natural Sciences, Bahcesehir University, Istanbul, Turkey
[i] Faculty of Science and Letters, Piri Reis University, Tuzla, Istanbul, Turkey
[j] Department of Computer Science and Engineering, The NorthCap University, Gurgaon, Haryana, India

ARTICLE INFO

Keywords:
Incremental learning
Cascaded Model
Tuberculosis (TB)
FRCNN
Chest X-Ray
Radiology

ABSTRACT

Rapid treatment protocols such as X-ray and CT scans have played a crucial role in the diagnosis of tuberculosis (TB infection). Automatic detection of CXR is required to speed up patient treatment with accuracy. Consequently, it reduces the burden of patients on medical practitioners. The present paper proposes an incremental learning-based cascaded (ILCM) model to detect tuberculosis from Chest X-ray images. The proposed model also localizes the infected region on the CXR image. The experimental outcome, clearly indicates that the performance is better than the pre-trained model as tested on the local population data (93.20% overall accuracy), F1 score of 97.23% (harmonic mean of precision and recall). Where the Golden standard dataset was 83.32% overall accuracy, and F1 score 82.24%.

1. Introduction

Ten million people contract the virus each year, and 1.45 million people die from tuberculosis (TB). The World Health Organization (WHO) reports that South-East Asia has the highest prevalence of tuberculosis (44 %), followed by Africa (24 %), the Western Pacific (18 %), the Eastern Mediterranean (8 %), North America (3 %), and Europe (3 %). One and a half million people, or 15 %, of the seven million individuals recorded in 2018, have no symptoms of TB. This indicates that using bacterial approaches to diagnose these patients is challenging. However, only a maximum of 70 % of the 5.9 million individuals with pulmonary TB have had their illnesses confirmed bacteriologically in recent years. The remaining cases were then given a clinical diagnosis based on the symptoms, abnormalities on the chest X-ray (CXR), and the patient records. In this situation, a prompt and precise diagnosis would be crucial for the treatment and management of the illness. The method for isolating bacteria continues to be the gold standard for case determination tests. The approach has a somewhat low sensitivity despite having a very high specificity. Additionally, such a test is a lengthy procedure that could take at least three weeks to provide the results.

Testing methods used in immunology and molecular biology each have advantages and limitations of their own. The drawbacks of the two procedures outlined above are essentially overcome by the Polymerase Chain Reaction (PCR) technique used to examine the molecular markers of TB in patient samples. Unfortunately, because PCR procedures are so expensive, not all medical facilities can use them. Pre-screening facilities

* Corresponding authors at: Decisions Lab, Mediterranea University of Reggio Calabria, Reggio Calabria, Italy (A. Ahmadian), Faculty of Engineering and Natural Sciences, Istanbul Okan University, Istanbul, Turkey (S. Salahshour), Department of Computer Science and Engineering, The NorthCap University, Gurgaon, Haryana, India (A. Katti).

E-mail addresses: svats@gehu.ac.in (S. Vats), vsharma@gehu.ac.in (V. Sharma), karan@mail.jnu.ac.in (K. Singh), anveshakatti@gmail.com (A. Katti), mazeyanti@utp.edu.my (M. Mohd Ariffin), mnazir@ukm.edu.my (M. Nazir Ahmad), ahmadian.hosseini@unirc.it (A. Ahmadian), soheil.salahshour@eng.bau.edu.tr (S. Salahshour).

https://doi.org/10.1016/j.eswa.2023.122129
Received 8 November 2022; Received in revised form 8 September 2023; Accepted 10 October 2023
Available online 14 October 2023

Table 1
COMPARISON OF EXISTING STATE-OF-THE-ART MODELS.

Model	Methodology	Dataset	Accuracy (%)	Accuracy (Local population)	Accuracy (Demographic population)
(Tabik et al., 2020)	Covid-SDNet, combines the segmentation, data augmentation, and transformation concept	COVIDGR 1.0 (Contains CXR and RT-PCR)	97.00 %	✓	–
(Ismael & Şengür, 2021)	SVM based classifier	380 CXR Images (Covid-19 and Normal)	92.06 %	✓	–
(Hussain et al., 2021)	CoroDet CNN-based model (22 layers of CNN)	COVID-R dataset (7390 of CT and CXR)	99.00 %	✓	–
(Afshar et al., 2020)	COVID-CAPS-Capsule Networks	NIH Dataset (112,120)	98.01 %	✓	–
(Taresh et al., 2021)	Transfer learning	2700(Covid and Non Covid)	98.01 %	✓	–
(Dansana et al., 2023)	Transfer learning (VGG-19)	Pneumonia (360)	91.02 %	✓	–
(Kc et al., 2021)	Transfer learning	Covid (760)	96.02 %	✓	–
(Sitaula & Hossain, 2021)	Attention-based VGG-16	Dataset (375)	79.02 %	✓	–

are urgently required in the given situation to carry out early diagnosis. Monitoring TB with the aid of medical imaging tools, among other things, is beneficial to the diagnosis and prognosis of the illness. X-ray has been an effective tool to visualize the organs under the skin and flesh without physically reaching the organ. In the present work, an incremental learning-based intelligent system to detect and localize the infection caused by TB has been proposed. It uses a multi-layered approach to diagnose the infection and recursively learns the behaviour and impacts of the TB variants of the new kind. The article is divided into six sections. In section 2, the literature review is done based on different models utilized for disease identification. In section 3 ILCM (Incremental learning-based cascaded Model) model is proposed with its workflow. Section 4 defines the different datasets utilized for the training and testing of the ILCM model. Section 5 provides experimental analysis and result discussion followed by the conclusion in section 6.

2. Literature review

Artificial intelligence (AI) has recently become more prevalent in many facets of daily life and has led the way in approaches used to enhance goods and services. Numerous methods have been implemented to help doctors with their daily responsibilities as the use of AI and Deep Learning in healthcare is increasing. Numerous research already in existence have shown how AI can speed up disease detection. Particularly, models created on top of Deep Learning algorithms yield increasingly accurate findings, advancing the application of AI to interpret medical pictures and particularly to detect TB from CXR images. Numerous research studies have been conducted regarding lung cancer detection (K. Santosh et al., 2022; K. C. Santosh & Antani, 2018).

Due to the pandemic, automatic detection of CXR disease is required to speed up patient treatment and reduce the burden on medical practitioners. In this digital era, devices (mobile phones, digital sensors, communications devices, etc.) have abilities to generate huge amounts of data such as structured, semi-structured, and unstructured growing exponentially with time. Various researchers adopt the deep learning method (CNN-Convolution Neural Network provides an effective method for the identification and classification of digital images) to find the covid-19 abnormality using chest X-Ray (CXR) and CT-Scan images, with the help of pre-trained models (Aboutalebi et al., 2021; Adimoolam et al., 2022; Afshar et al., 2020; Albahli, 2020; Apostolopoulos & Mpesiana, 2020; Chowdhury et al., 2020; Civit-Masot et al., 2020; Dansana et al., 2023; El Asnaoui & Chawki, 2020; Farooq & Hafeez, 2020; Fouladi et al., 2021; Hemdan et al., 2020; Hussain et al., 2021; Ismael & Şengür, 2021; Jacobi et al., 2020; Kc et al., 2021; Khan et al., 2020; Kumar Sethy et al., 2020; Maghdid et al., 2021; Mahbod et al., 2019; Minaee et al., 2020; Narin et al., 2020; Ozturk et al., 2020; Punn & Agarwal, 2021; Sitaula & Hossain, 2021; Tabik et al., 2020; Taresh et al., 2021; Vaishya et al., 2020;),(Henderson & Santosh, 2023; Mahbub, Biswas, et al., 2022; Mahbub, Hossain Zamil, et al., 2022; Mukherjee et al., 2021; Roy & Santosh, 2023; K. Santosh et al., 2022; K. C. Santosh, 2020b; 2020a; K. C. Santosh et al., 2016, 2022; K. C. Santosh & Antani, 2018; K. Santosh & Ghosh, 2021).

The COVIDGR 1.0 database, which is utilized datasets from Sancecilio, Granda, and Spain. This dataset represents all levels of severity of RT-PCR (including normal and positive RT-PCR cases). COVIDGR 1.0 also contains CXR Images (PA view- 426 normal and 426 positive cases). They use the covid-SDNet (Covid Smart Databased Network) methodology on COVIDGR 1.0, to improve the generalization aspect of the classification model. Covid-SDNet, combines segmentation, data augmentation, and transformation concepts. The author achieved an accuracy of 97 %, 86 %, and 61 % for severe, moderate, and mild covid-19 respectively, which shows good generalization capacity of covid-SDNet. The utilized methodology of the covid-SDNnet performed well on COVIDGR 1.0, but it is not mentioned the demographic accuracy (Tabik et al., 2020). CoroDet CNN-based model, which classifies covid-19 using CXR and CT-scan. CoroDet has utilized 22 layers of CNN models. It uses the COVID-R dataset, in which 7390 CT and CXR (Covid-2843, Normal-3108, and Pneumonia (Viral + Bacterial) −1439) are involved in building CoroDet. It can classify up to four classes such as COVID, NORMAL, Non-COVID Viral pneumonia, and non-Covid bacterial pneumonia. The author tested CoroDet performance in three ways, it gives 99 %, 94.2 %, and 91 % accuracy for two classes (Covid and Normal), three (Covid, Normal, and Non-Covid pneumonia), and four classes (Covid, Normal, Non-Covid, Viral pneumonia and Non-Covid bacterial pneumonia, respectively). The outcome of this study indicates the superiority of CoroDet as compared to the existing state-of-the-art. The utilized methodology (CoroDet) on the given dataset performed well but, has not mentioned the demographic accuracy (Hussain et al., 2021), as shown in Table 1.

SVM-based classifier with different kernel functions such as quadric, cubic and gaussian is used to identify covid-19 disease. In which, the epsilon value of the quadratic and linear kernel function is set at 0.04 and 0.02, and the cubic and Gaussian function's value is set at 0.01. They have performed fine-tuning on the different pre-trained models (Ismael & Şengür, 2021).

3. Contribution

The present model is the introduction of a progressive learning-based method, where an X-Ray image is processed through multiple stages to identify and localize the tuberculosis disease. The prime features of the proposed models are as follows.

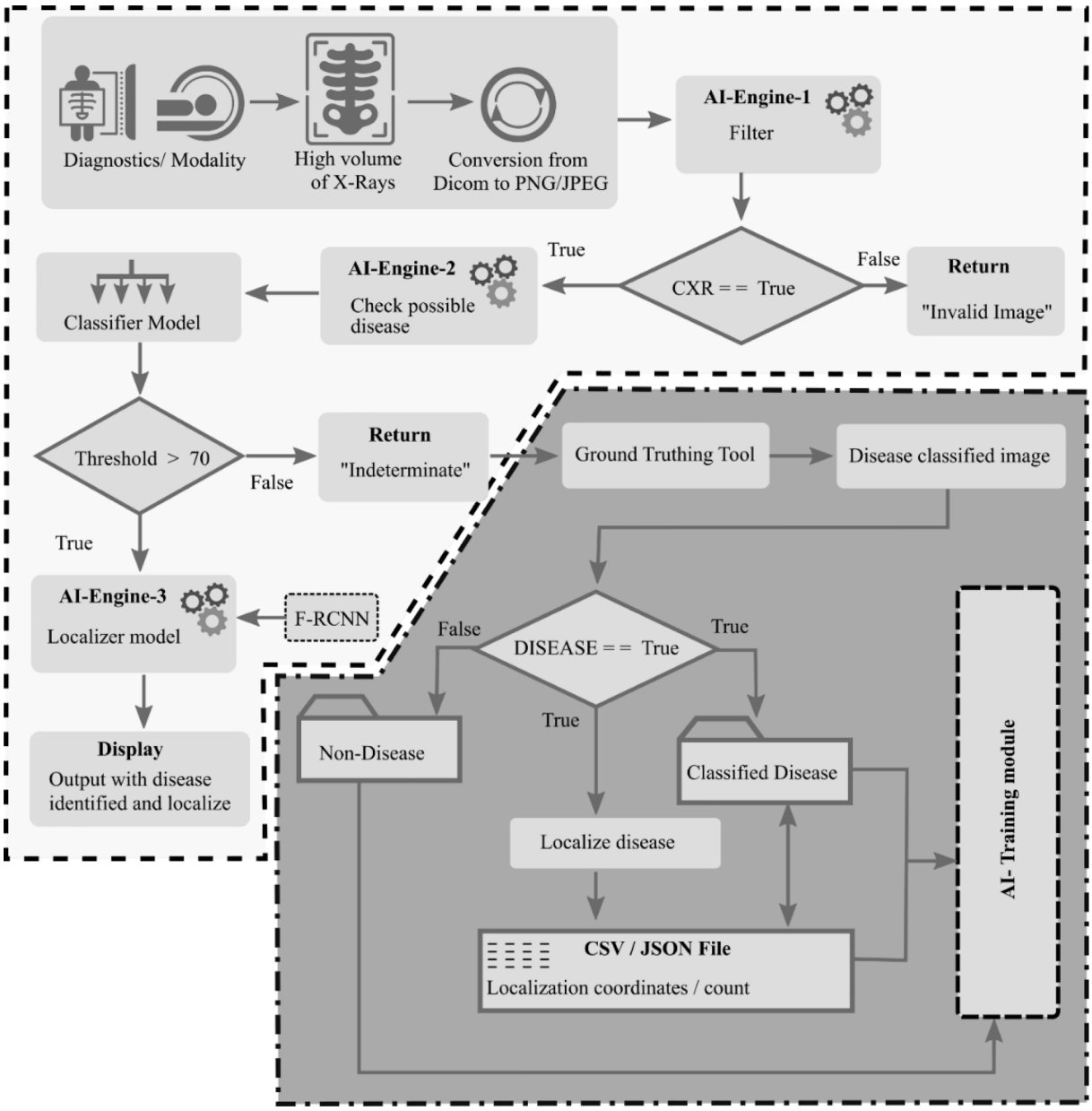

Fig. 1. Testing (AI Engine 1, 2, and 3) and GT-Tool workflow.

1) It uses the multi-layered cascaded model to pre-process the images before they are passed to the classifier and localizer.
2) It is an auto-learning iterative model, which is designed to enhance its accuracy and ability with experience.

4. Proposed model: Ilcm

AI uses deep learning and neural network techniques to detect various diseases in CXR. There are numerous associated functions in a neural network, which have weight and bias factors. A network's operation is modelled after how the human brain functions. Deep learning contains several hidden layers that train networks using known positive and negative examples (ground reality). The weights and biases in the underlying function assist the network in learning back-propagation, which is based on the variances between forecast and actuality. A deep learning network can adapt and train itself using enormous training datasets, which allows it to recognize new and unseen data. It employs AI techniques to categorize the possible cases as TB illnesses. Its primary goal is to support physicians in achieving better and improved clinical results. The current AI model provides various health sector supports to identify various ailments. It may interface with an X-ray machine and use the CXR images as input for its AI engine (that uses deep learning and neural networks) to identify the various disorders in CXR.

With the use of several CXRs, this AI engine has been trained to identify potential TB sickness. More CXR images (as a dataset) will result in better and more accurate clinical results because machine learning and deep learning tasks are resource-hungry. After the current AI model has analysed the CXR images, a prioritized list is displayed on the doctor's screen. The burden and time required for radiologists to manually read CXR images are undoubtedly reduced by the integration of AI technology with the X-ray machine to analyze the CXR images.

4.1. Working

In the proposed model three AI engines such as AI-1, AI-2, and AI-3 were used to filter (CXR & Non_CXR), disease classification, and disease localization, respectively. X-Ray generated from the modality M is

directly send to X-Ray DICOM converter unit, which converts the DICOM X-Ray image to the JPEG/PNG format. This format can be easily utilized in machine learning training.

An incremental learning-based cascaded approach is introduced, so that when an X-Ray image comes from the DICOM converter, it sends for filtration (CXR and Non_CXR), disease classification, and disease localization by using AI-1, AI-2, and AI-3, respectively (Fig. 1). Converted X-Ray passes on AI-1 (Filter- based on sigmoid activation function) and CXR==True, and on AI-2 for disease classification. In AI-2 (based on SoftMax activation function), when the threshold value is less than 70, the CXR are sends for the ground-truthing with the help of GT-Tool, managed by the senior radiologist. The returned output of the same is indeterminate. Once AI-2 receives the threshold value greater than 70, the AI-3 multi-disease classifier (enabled by the SoftMax activation function) classifies the disease and sends that CXR for disease localization, with the help of faster-RCNN.

Instead of transfer learning, the trained neural network from scratch, we have created our own defined custom hidden layers using functional API (TensorFlow - Keras). The research-based calibrated architecture of the neural network was defined and the input data was fed into its input layers. The data flows from input layers to custom-defined hidden layers and finally through the output layer of the neural network. After the completion of the forward loop of the network, backward data propagation takes place, when the computational error rate is adjusted as per derivatives of error (including gradient & step size), and updates in weights & bias of each layer to reduce the error rate. The above-mentioned process is iterative, while learning a custom-defined neural network. In this way, two important phases are involved during training for CNN. (1) Forward Propagation phase: which includes three major tasks- a) Receive input data, b) process the information, and c) generate the desired output. (2) Backward Propagation phase: which includes two major tasks– a) Calculate errors while learning, b) Update the parameters of the CNN. The mathematical representation for Forward Propagation at the Convolution Layer is as follows:

$$Z = X*F \tag{1}$$

Here in equation (1), symbol * (asterisk) denotes the Convolution. The F symbol denotes the Filter, and the Z symbol denotes the input images. The next step is to apply the activation function – here Sigmoid Function is used (see equation (2).

$$A = sigmoid(Z) \tag{2}$$

Now, Linear Transformation is applied to the values (randomly initialized weight and bias matrix), see equation (3).

$$LT = WA + B \tag{3}$$

Where, LT (equation (3) represents the Linear Transformation, W stands for randomly initialized Weight, and B stands for randomly initialized Bias. The "Sigmoid" Function is applied to the dataset to generate the final output of the neural network. Mathematically represented as equation (4).

$$O = Sigmoid(LT) \tag{4}$$

Where O (equation (4) stands for the final Output of the Neural network.

The mathematical representation for backward propagation at the convolution layer is given in Equation (5).

$$Parameter_{new} = Parameter_{old} - (Rate_{learning} * GradientDescent) \tag{5}$$

Here, the "gradient descent technique" for updating the parameters (equation (5). $Rate_{learning}$ is a constant value that controls the amount of change being made to old parameters. For updating the matrix, the gradient of the parameter such as – dE/dF (derivatives) is computed (equation (6). Here derivative values are also involved to update the filter value:

$$F = F - Rate_{learning} * \left(\frac{dE}{dF}\right) \tag{6}$$

4.2. Workflow info

Binary Classification (uses Sigmoid activation function) decides whether input images have an abnormality or not. If an abnormality is found, then it passes the image to the Multi-Class Classifier using the VGG network (SoftMax). FRCNN network uses the VGG-16 neural network for feature extraction from the input images. This task is completed using a stack of convolutional and "max pooling" layers. The last layer SoftMax multi-class classifier can be defined as equation (7):

$$\boldsymbol{F}(y = j|X_i) = \frac{e^{w_j X_i{}^T}}{\sum_{k=1}^{n} e^{\left(w_k X_i{}^T\right)}} \tag{7}$$

Here, X_i represents the feature vector that is extracted for the input image "i". W_i is the learning weight. And "y" represents the category of prediction, where j belongs to N (set of all labels).

In Equation (7), the SoftMax function is used to calculate the probability distribution over the different categories. The SoftMax function takes input from a vector of scores, and it outputs a vector of probabilities. The scores are calculated by multiplying the features by the weights of the fully connected layer. The probabilities are calculated by normalizing the scores so that they sum to 1.

Refinement is also done in the section on image contrast for better learning and localization purposes by establishing the relationship between the dark & light, and histo-graphic computation is done to correct the final pixel value, shown in equation (8).

$$\boldsymbol{RS}(x) = \sum_{y \in \Omega/x} \frac{S_a(I(x) - I(y))}{\|x - y\|}, x \in \Omega \tag{8}$$

where:
RS(x) is the refined pixel value at location x.
Sa is a weight that is assigned to each pixel y.
I(x) is the input grayscale image at location x.
I(y) is the input grayscale image at location y.
Ω is the set of all pixels in the image.
||x - y|| is the distance between the pixels × and y.

The refinement is done by establishing the relationship between the dark and light pixels in the image, and then correcting the final pixel value using a histogram computation.

The equation works by first calculating the difference between the pixel values at each location × and y. This difference is then multiplied by the weight Sa, which is a measure of how important the difference is. The weighted differences are then summed over all pixels y in the image. The final pixel value at location × is then calculated by dividing the sum by the distance between the pixels × and y.

The histogram computation is done to ensure that the final pixel values are distributed uniformly. The histogram of an image is a plot of the number of pixels at each grayscale value. The histogram computation ensures that the final pixel values are evenly distributed across the grayscale range. The refinement of image contrast is a common technique used to improve the visibility of objects in images. The technique is especially useful for images with many dark or light pixels.

The scaling of image enhancement is a common technique used to improve the visibility of objects in images. The technique is especially useful for images that have a large dynamic range, meaning that the difference between the minimum and maximum values of the image is large.

To improve the visibility of objects in images, image enhancement is applied. The technique is especially useful for images that have a **large dynamic range**, meaning that the difference between the minimum and maximum values of the image is large. mathematically represented as:

$$Q(x) = RS(x) - \frac{minRS}{(maxRS - minRS)} \tag{9}$$

where:

minRS is the minimum value of the image enhancement.

maxRS is the maximum value of the image enhancement.

Q(x) is the original pixel value at location x.

RS(x) is the enhanced pixel value at location x.

The equation works by first calculating the difference between the minimum and maximum values of the image enhancement. This difference is then used to scale all pixel values within the range of [0, 1]. The minimum value of the image enhancement is subtracted from all pixel values to ensure that all pixel values are positive. The final pixel value is then calculated by dividing the scaled pixel value by the difference between the minimum and maximum values of the image enhancement.

To reduce the error generated by the image enhancement process, the minimization of the error process is applied, where the goal is to minimize the error between the enhanced image and the original image.

$$theargmin \frac{1}{2}\sum_{x}\left(I(x) - \frac{1}{2}\right)^2 - \frac{1}{4M}\sum_{x}\sum_{y\neq x}\omega(x,y)St(I(x) - I(y)) \tag{10}$$

where:

I(x) and I(y) is the enhanced pixel value at location × and y.

5. Is a constant

4 M is a constant that depends on the size of the image.

6. Is the set of all pixels in the image

w(x, y) is a weight that is assigned to each pixel pair (x, y).

St is the difference between the pixel values at locations × and y.

In equation (10), the difference between the enhanced pixel value and the original pixel value at each location × is calculated. This difference is then multiplied by the weight w(x, y), The weighted differences are then summed over all pixel pairs (x, y) in the image. The final error is then calculated by dividing the sum by the number of pixel pairs.

The minimization (error) problem is resolved using an optimization algorithm, such as gradient descent. The optimization algorithm iteratively updates the parameters of the image enhancement model until the error is minimized.

Equation (11) defines the polynomial approximation of the slope function. The approximation is done by decomposing the slope function into a sum of convolutions. A convolution is a mathematical operation that combines two functions to produce a third function. In this case, the two functions are the slope function and a set of basis functions. The basis functions are typically chosen to be simple functions, such as sine and cosine functions.

$$RX(x) = \sum_{y\in T^2}\omega(x-y)\sum_{m=1}^{M} c_m(I(x) - I(y))^m$$

$$= -\sum_{y\in t^2}\omega(x-y)\sum_{m=1}^{M} c_m(I(x) - I(y))^m$$

$$= -\sum_{y\in t2}\omega(x-y)\sum_{m=1}^{M} cm\sum_{n=0}^{m}\binom{m}{n}I(y)^n(-I(x))^{m-n}$$

$$= \sum_{n=0}^{M}\left(\sum_{m=n}^{M} c_n\binom{m}{n}(-1)^{m-n+1}I(x)^{m-n}\right)\sum_{\substack{y\int T^2 \\ a \\ nx}}\omega(y-x)I(y)^n$$

$$= \sum_{n=0}^{M} a_n(x)(\omega^* I^n)(x) \tag{11}$$

where:

RX(x) is the polynomial approximation of the slope function at x.

w(x-y) is a weight function that determines the contribution of the convolution at location y to the approximation at location x.

C_m are the coefficients of the polynomial approximation.

I(x) is the input image.

y is a pixel location in the input image.

m is a polynomial order.

The weight function w(x-y) is typically chosen to be a Gaussian function. The Gaussian function is a bell-shaped function that falls off rapidly as the distance between × and y increases. This ensures that the convolutions only contribute to the approximation at nearby locations. The coefficients C_m are determined by solving a least squares problem. The least squares problem minimizes the error between the polynomial approximation and the slope function. The polynomial approximation of the slope function can be used to improve the performance of image processing algorithms. For example, it can be used to smooth images, remove noise, and enhance edges.

Equation (12) defines the working for interpolation using the discrete cosine transformation with boundary handling. The interpolation is done by first computing the discrete cosine transform of the input image. The discrete cosine transform is a mathematical operation that decomposes a signal into a sum of cosine functions. The coefficients of the discrete cosine transform are then used to reconstruct the image at any desired location.

$$RX(x;L) = \sum_{y\in T^2}\omega(x-y)St(L - I(y)) \tag{12}$$

Where:

RX(x; L) is the interpolated image at location × and size L.

w(x-y) is a weight function that determines the contribution of the pixel at location y to the interpolation at location x.

St (L - I (y)) is the discrete cosine transform of the pixel at location y.

The boundary handling is done by using a special algorithm that ensures that the reconstructed image is smooth at the edges. The algorithm typically uses a combination of zero-padding and extrapolation. Zero-padding is the process of adding zeros to the edges of the image before computing the discrete cosine transform. Extrapolation is the process of estimating the values of the image outside the boundaries using the values of the image inside the boundaries.

Equation (12) is a powerful technique that can be used to improve the visibility of objects in images. The technique is especially useful for images that have a lot of noise or that are low in contrast. By equations (7) to (12), the object detection process is enhanced, which is responsible for improving the accuracy of the FRCNN algorithm.

There are two types of activation functions used in machine learning and deep learning, The first is the Linear activation function, which is a function represented by a line or linear equation. Mathematically represented as (Equation): f(x) = x where the range is defined as: (-infinity to infinity). The second one is non-linear activation functions; these functions are the most used activation functions in the domain of deep learning. The sigmoid function is a kind of non-linear activation function, and it is represented by a curve that looks like an S-shape.

The main reason to use the sigmoid function comes from its existence between (0 to 1). Hence, it can be used for AI models to determine or predict the probability as an output of a dedicated AI model (AI Engine-1). The probability exists only in between the range of 0 and 1, therefore sigmoid function becomes the right choice for binary classification problems handled by CNN. Hence, the slope of the sigmoid (S-shape) curve can be determined at any two points. The sigmoid function is a better option to deal with binary classification problems in the machine learning domain. Whereas, in the multiclass classification problem, the

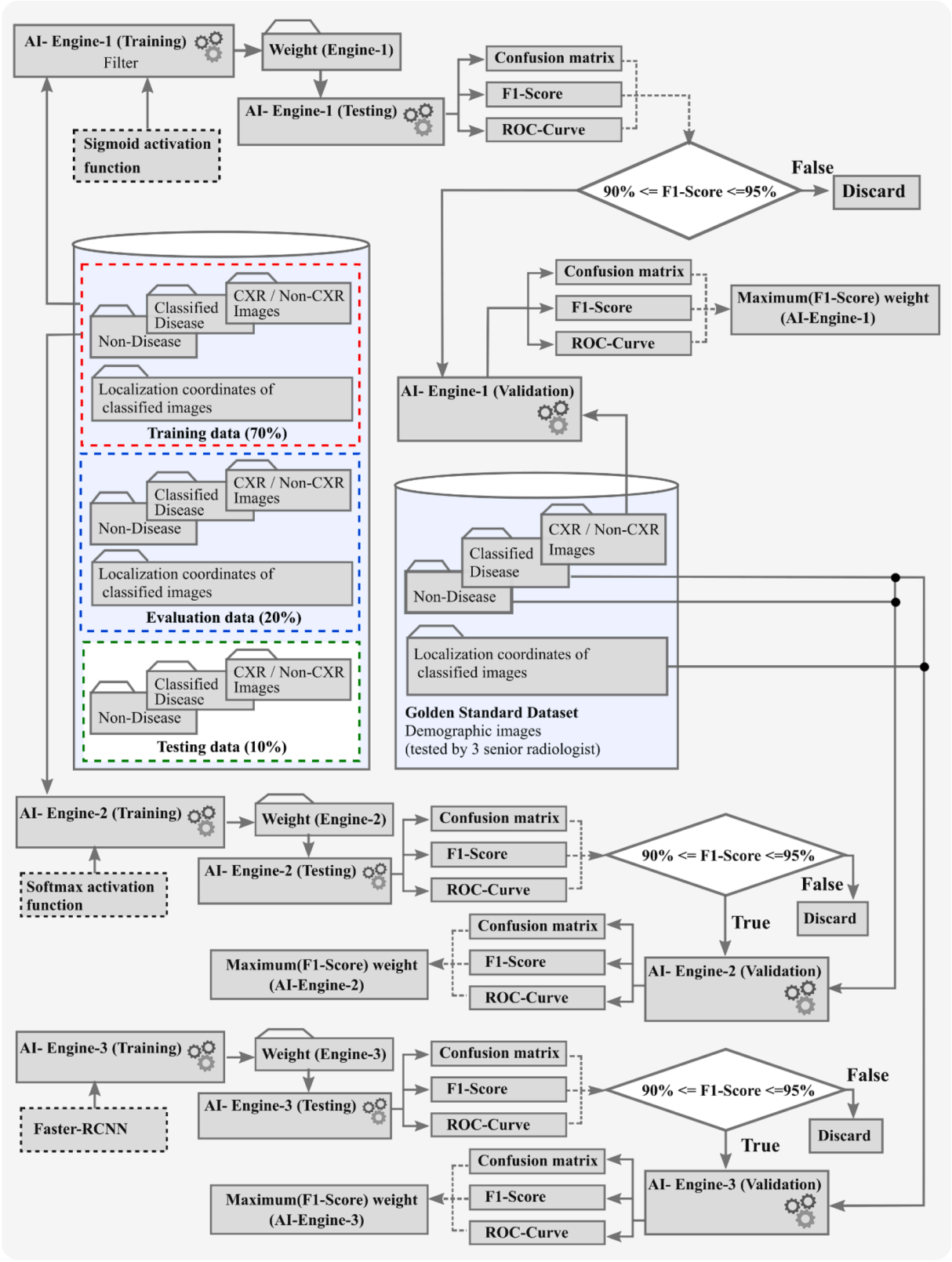

Fig. 2. Training (AI Engine 1, 2, and 3).

SoftMax function is the better choice as it returns each class's probability. A mathematical representation of the SoftMax activation function is provided below in equation (13):

$$Softmax(z_i) = \frac{exp(z_i)}{\sum_j exp(z_j)} \tag{13}$$

The Z symbol represents the values from neurons of the output layer and the exponential acts as the non-linear function. Later these values

are also divided by the "sum of exponential values" for normalization and finally converted into values of probabilities.

Algorithm:1

Diagnostic/Modality → M
AI → AI Engine (Weight)
W- Weight (Trained Model)
Chest X-Ray → CXR
Filter (CXR and other X-RAY) → AI-1
Disease Classification → AI-2
Disease Localization → AI-3
DS → Data Set (Training (70 %) / Evolution (20 %) / Testing (10 %))
GS → Golden Standard Dataset (Demographic).
GT-Tool → Ground Truthing Tool

Testing Phase
1- *Modality (M) → Generates X-Ray (DICOM) → Converter == X-Ray (JPEG/PNG)*
2- *X-Ray → AI-1 (Filter for CXR)*
If (CXR == False)
Return invalid image;
Else
*Send CXR → AI-2 /**For Disease classification***
If (Threshold > 70)
*Send CXR → AI-3 /**Localize the disease***
Return Localize and Disease classified CXR image;
Else
Send CXR → GT- Tool
Return Indeterminate;
3- *GT- Tool → Identification of Disease in CXR /**BY Radiologist***
If (Disease == False)
*Send CXR → Store in Non_Disease class; /**Further Training***
Else
Disease with Localization → CXR;
Store in DS (identified Class) → CXR;

Training Phase
4- *DS → Non_Disease / Disease classified and localized coordinates /**Filter (CXR/ Non_CXR)***
4A: *Non_CXR (DS) → AI-1 (Training)*
If (F1 Score ≥ 90 % && ≤ 95 %)
Sends W → GS (Validation Testing);
Store W → Max (F1 Score);
*Update (W) = AI-1 (Training) → AI-1 (Testing); /**On Step 2***
Else
Discard W;
4B: *Disease_Class (DS) → AI-2 (Training)*
If (F1 Score ≥ 90 % && ≤ 95 %)
Sends W → GS (Validation Testing);
Store W → Max (F1 Score);
*Update (W) = AI-2 (Training) → AI-2 (Testing); /**On Step 2***
Else
Discard W;
4C: *Disease_Class (DS) → AI-3 (Training)*
If (F1 Score ≥ 90 % && ≤ 95 %)
Sends W → GS (Validation Testing);
Store W → Max (F1 Score);
*Update (W) = AI-3 (Training) → AI-3 (Testing); /**On Step 2***
Else
Discard W;
5- *Return output as Disease identified and localized;*

GT-tool is operated by senior radiologists, which classify possibilities with their localized coordinates. The classified and localized disease in the CXR verified by the GT activity is then stored in dataset DS, where they are involved in training (70 %), evaluation (20 %), and testing (10 %) as shown in Fig. 2. Each AI engine (AI-1, AI-2, and AI-3) is maintained as separate training mechanism, which directly fetches their respective data belonging to the labelled class from DS.

Since the training is not a routine process of proposed model (ILCM), it is done extensively in the beginning, when the bulk amount of data is provided to the model for the initial training process. Subsequently, the model is updated at irregular intervals, when new labelled dataset is available. The decision of updating ILCM is based on the equation (14).

Table 2
Dataset Description.

Link	DATASET NAME	IMAGES
(*Tuberculosis Chest X-Rays (Shenzhen)* | *Kaggle*, n.d.)	Tuberculosis Chest X-rays (Shenzhen)	662 PNG
(*Drug Resistant Tuberculosis X-Rays* | *Kaggle*, n.d.)	Drug-resistant tuberculosis X-rays	1047 DCM (DICOM)
(*Index of Public/Tuberculosis-Chest-X-Ray-Datasets/Montgomery-County-CXR-Set/MontgomerySet/*, n.d.)	Montgomery County	400 files
(Rahman et al., 2020)	TUBERCULOSIS	7000 images
(Zaidi et al., 2022)	NIH Chest X-rays	112 k images in the dataset and 47,697 (TB)

$$Update(model) = \begin{cases} True, IfsizeOf(dataset) > threshold_{update} \\ False, Otherwise \end{cases} \quad (14)$$

where is the value of $threshold_{update}$ is 100 for the proposed model,

The testing phase of the model is significant as it is meant to be used by the modality to classify each generated X-RAY image.

The complexity of the ILCM is $O(n^2m^2)$, where $(n \times n)$ is the resolution of CXR image fed to the first convolutional layer and $(m \times m)$ is the dimension of the kernal function.

In the training phase, for the model accuracy, two tests where performed. The first one is tested using a CXR image, which is stored in DS and maintained by the 10 % (Not involved in training) records of the total dataset. Second testing, named validation testing, here a demographic (Golden Standard) dataset containing TB diseases are gathered from different geographical locations/ hospitals across the globe (shown in Fig. 2). In the validation test, the correct weight (Model) can be obtained by the calculation of the maximum F1-Score. Once the updated weight from the validation testing for all three AI engines is procured, then it is directly updated in the testing phase as mentioned in the algorithm and shown in Fig. 1. The outcome can be shown in the form of the testing phase that disease is identified and localized.

7. Datasets

Several datasets of the TB disease have been used in the present experimental study. The Golden standard dataset from the different demographic locations was also maintained.

A "golden standard dataset" refers to a collection of data that is considered to be the most reliable and accurate representation of a particular phenomenon or population. It is the ideal dataset that researchers strive to use as a reference or benchmark for their studies. When this golden standard dataset is collected from different demographic locations, it means that the data has been gathered from a variety of places with different characteristics, such as age, gender, ethnicity, education level, income, geographic location, and so on. With the help of datasets from diverse locations, scientists can get a more inclusive understanding of the phenomenon they are reviewing, and they can ensure that their findings are not biased towards any group or region. Data from a range of locations, researchers can better understand how health problems vary across different demographics, and they can develop interventions and policies that are more effective at improving public health outcomes for all populations.

The golden standard dataset consists of 4000 CXR (2000 TB and 2000 non-TB) maintained demographically(Chowdhury et al., 2020; *COVID-19 Radiography Database* | *Kaggle*, n.d.; *Files - BSC B2DROP*, n.d.-a; *Files - BSC B2DROP*, n.d.-b; *Index of Public/Tuberculosis-Chest-X-Ray-Datasets/Montgomery-County-CXR-Set/MontgomerySet/*, n.d.; *Tuberculosis Chest X-Rays (Shenzhen)* | *Kaggle*, n.d.; Rahman et al., 2020; Zaidi et al., 2022), (*Chest Xray Masks and Labels* | *Kaggle*, n.d.; *NIH Chest X-Ray Dataset* | *Cloud Healthcare API* | *Google Cloud*, n.d.; Dinesh Jackson

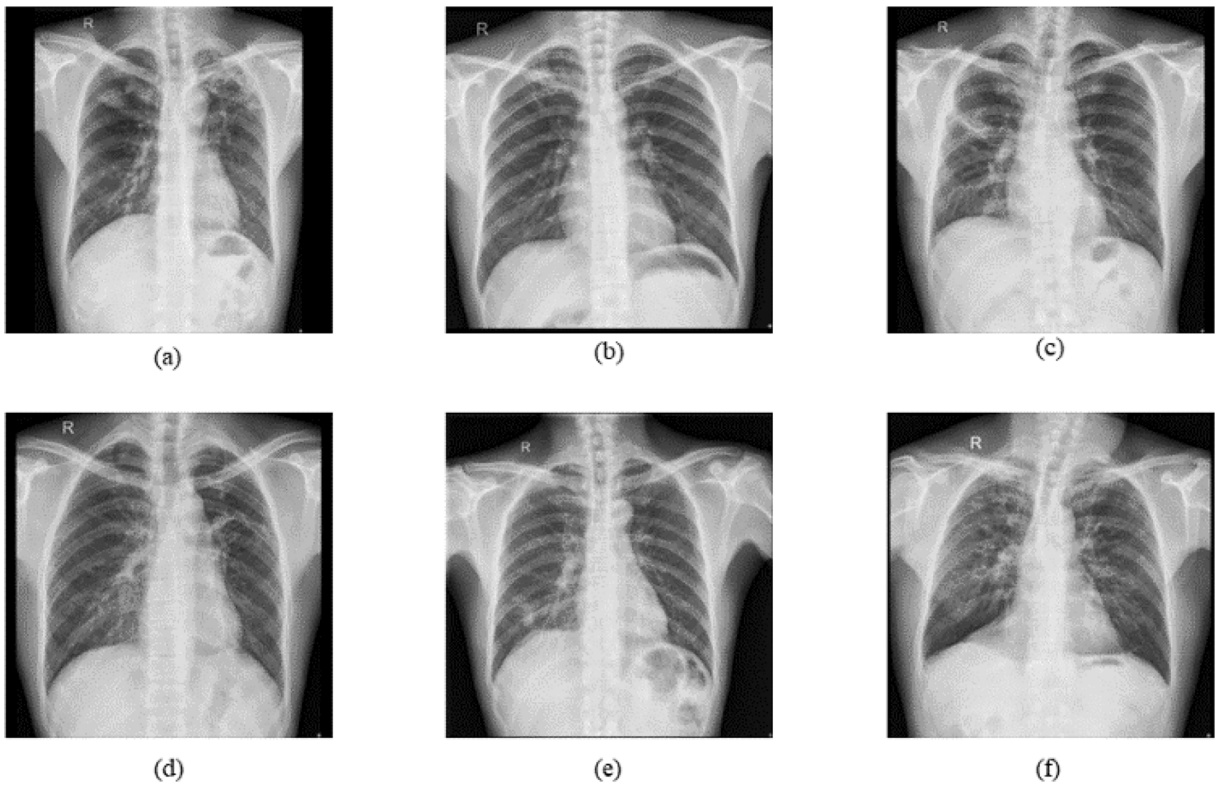

Fig. 3. Sample TB CXR images.

Samuel & Rajesh Kanna, 2019; Jaeger, Candemir, et al., 2014; Jaeger, Karargyris, et al., 2014; Pande et al., 2016). Five thousand good quality CXR (collected from five different sources, mentioned in Table 2 with sample images Fig. 3) were used in the training process. The outcome of the training is then validated on a golden standard dataset verified by three radiologists.

The first Dataset Consists of 662 PNG files and one CSV file, providing information about patients diagnosed with tuberculosis in the region of Shenzhen, China. This dataset provides valuable insights into the prevalence of TB and its impact on patients. It consists of four columns, including study ID, sex, age, and findings. There are 662 unique values in the study ID column, with males accounting for 69 % and females for 31 % of the dataset. The age column ranges from 1 to 89 years old, with the middle-aged population being the average age. The findings column indicates that 49 % of patients were diagnosed as normal, 9 % with bilateral PTB, and 42 % with other conditions.

The second Dataset Consists of data on patients who developed resistance to conventional tuberculosis treatment. The data is available in raw format from https://tbportals.niaid.nih.gov and mainly represents the population of Belarus, with over 1000 tuberculosis cases. The dataset comprises 1049 files, including 1047 DCM files, one CSV file, and one other file. It features six columns, including filename, which has 1048 unique values, study_id, which has 1044 unique values, patient_-identifier ranging from 72 to 1229, gender, with males accounting for 62 % and females for 38 %, and TB_localization, with 51 % indicating pulmonary tuberculosis and extrapulmonary tuberculosis, and 49 % indicating pulmonary tuberculosis only.

The Third Dataset Consists of information from X-rays gathered as part of Montgomery County, Maryland's tuberculosis screening program. This dataset includes 400 PNG files and a filename column with 1044 unique values, as well as text files that provide information on the patient's sex, age, and abnormality of the lung. Of the total cases in the dataset, 58 show a manifestation of tuberculosis, while 80 cases are considered normal.

The fourth Dataset Consists of a chest X-ray image dataset for tuberculosis (TB) positive cases and normal images. This data was gathered as a collaboration between researchers of Qatar University, Qatar, Doha, Bangladesh, the University of Dhaka, Hamad Medical Cooperation and some researchers from Malaysia. The current release of the dataset comprises 3500 TB images and 3500 normal images,

Table 3
Testing Accuracy (DS and Maintained by 10% (Not involved in training).

Model	Accuracy	F1	MCC	Precision	Specificity	Sensitivity
AlexNet	0.8445	0.8258	0.8535	0.8812	0.8185	0.8845
GoogLeNet	0.8608	0.8306	0.8406	0.8972	0.8873	0.8712
VGGNet-16	0.8123	0.8153	0.8553	0.8143	0.8871	0.8854
ResNet-50	0.8621	0.8702	0.8730	0.8102	0.8345	0.8452
Inception V3	0.8725	0.8456	0.8345	0.8567	0.8456	0.8671
Xception	0.8754	0.8612	0.8425	0.8125	0.8456	0.8425
InceptionResNet V2	0.8526	0.8526	0.8456	0.8452	0.8453	0.8454
Mobile NET	0.8745	0.8726	0.8734	0.8734	0.8765	0.8752
DenseNet 169	0.8426	0.8351	0.8462	0.8325	0.8461	0.8426
NasNetLarge	0.8925	0.8952	0.8954	0.8925	0.8935	0.8945
DenseNet 121	0.8324	0.8452	0.8256	0.8354	0.8452	0.8342
ILCM (Proposed)	0.9320	0.9723	0.9826	0.9712	0.9721	0.9723

Table 4
TESTING ACCURACY (DEMOGRAPHIC).

Model	Accuracy	F1	MCC	Precision	Specificity	Sensitivity
AlexNet	0.6214	0.5912	0.5525	0.6110	0.5126	0.5826
GoogLeNet	0.6108	0.6306	0.6406	0.6325	0.6256	0.6135
VGGNet-16	0.5723	0.5625	0.5714	0.5912	0.6125	0.6258
ResNet-50	0.6125	0.6285	0.6358	0.6458	0.6245	0.6358
Inception V3	0.6532	0.6451	0.6452	0.6325	0.6345	0.6435
Xception	0.6245	0.6712	0.6645	0.6625	0.6725	0.6825
InceptionResNet V2	0.6524	0.6874	0.6572	0.6845	0.6425	0.6354
Mobile NET	0.6264	0.6625	0.6425	0.6356	0.6452	0.6525
DenseNet 169	0.6325	0.6452	0.6523	0.6645	0.6652	0.6645
NasNetLarge	0.6354	0.6521	0.6548	0.6354	0.6457	0.6412
DenseNet 121	0.6326	0.6546	0.6654	0.6754	0.6324	0.6452
ILCM (Proposed)	0.8332	0.8224	0.8528	0.8357	0.8445	0.8656

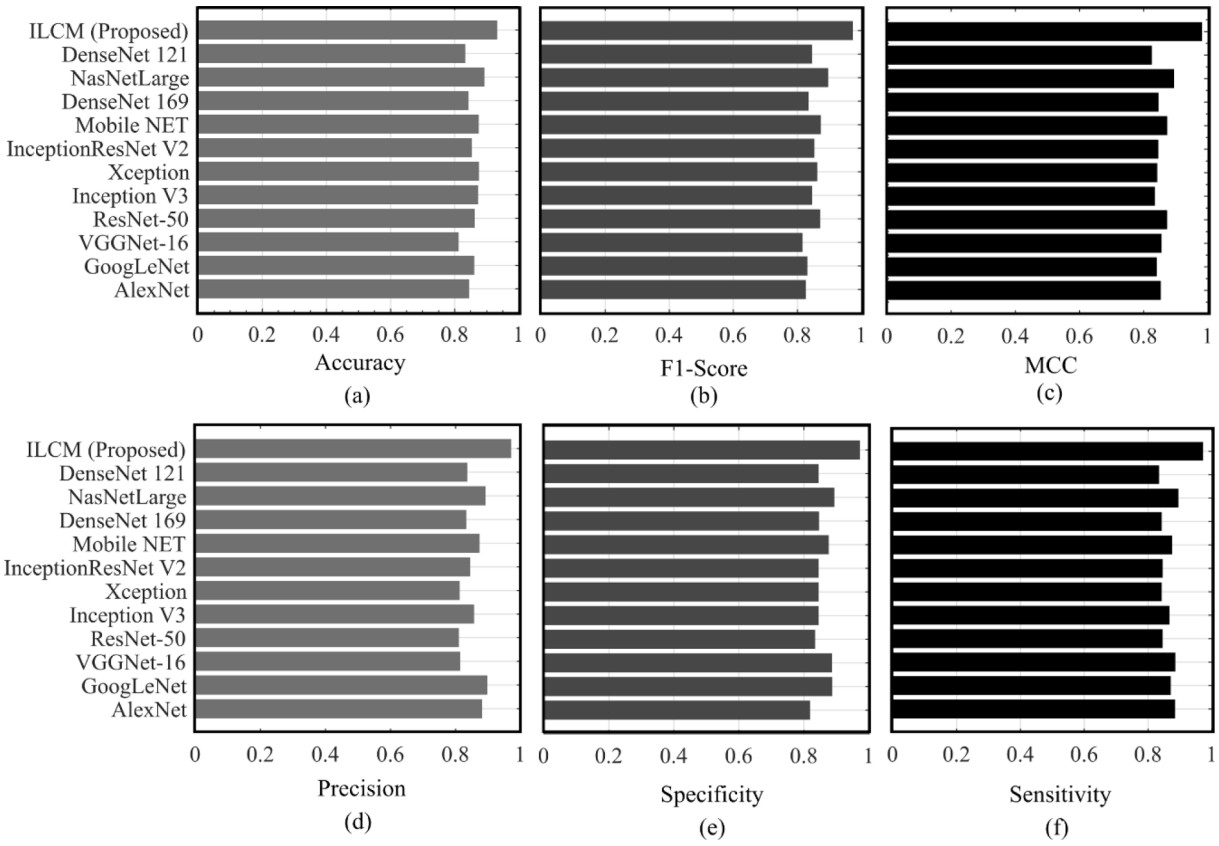

Fig. 4. Testing Accuracy (DS maintained by the 10% (Not involved in training).

providing a comprehensive resource for researchers.

The Fifth dataset consists of over 100,000 chest X-ray images with disease labels, including tuberculosis. The dataset was produced to aid in the development of chest X-ray-based, clinically useful computer-aided detection and diagnosis (CAD). Natural Language Processing (NLP) was used to produce the disease labels to derive disease classifications from the related radiological reports. The authors estimate that the labels are over 90 % accurate. While the dataset contains labels for multiple lung diseases, 47,697 images were labelled with tuberculosis-related manifestations such as atelectasis, effusion, pneumonia, nodule, consolidation, pneumothorax, emphysema, fibrosis, pleural thickening, and infiltration. These images were separated from the dataset and treated as infected images to focus on tuberculosis detection. A deep learning approach was used to predict the occurrence of each tuberculosis manifestation from the infected chest X-ray images, treating each manifestation as a separate class.

8. Result and discussion

The complete existence of the present model is measured by the False Negative/ False Positive/ True Negative/ True Positive four guidelines of the confusion matrix. False Negatives and False Positive could deviate the medical/clinical decision negatively. The False Positive diagnosis of TB may expose the individual to the TB potential. Similarly False Negative is expected to be part of TB patients instead of excluded from the TB-infected class. The performance of the proposed model is evaluated based on accuracy, F1 score, precision (PPV), specificity (SPC), sensitivity (SEN), and Mathew correlation coefficient (MCC).

Monitoring of the above guidelines for outcome as given in Table 3, is done with the help of different pre-trained models such as Alex Net, Google Net, Resnet-50, VGG-16, Inception V3, Xception, InceptionResNet V2, Mobile NET, DenseNet 169, NasNetLarge, and DenseNet 121. Then pre-trained models were used for comparative analysis on 10 % of the data, which is not involved in the training. Table 3 demonstrated

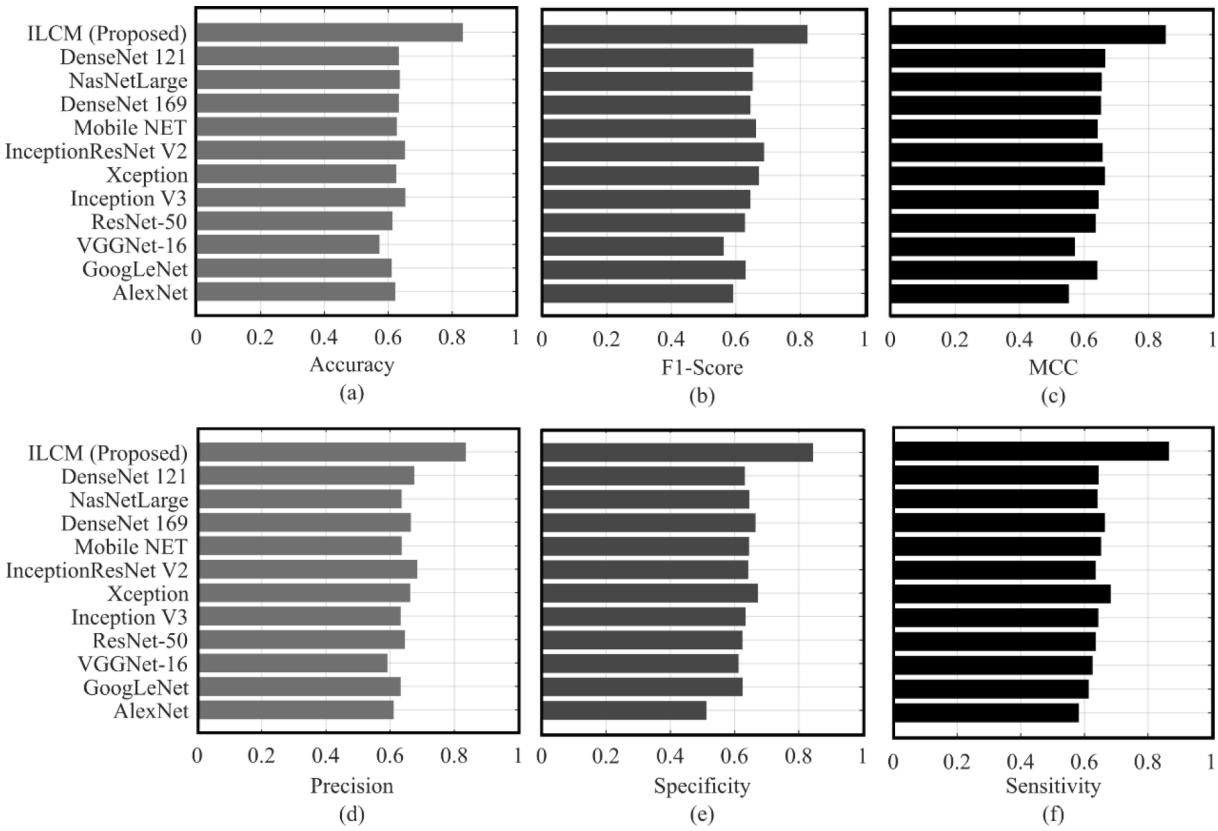

Fig. 5. Testing Accuracy (Demographic).

that the ILCM model performs well in identifying and localize the diseases. Similarly, a comparative analysis based on the demographic data set (Golden Standard dataset) was taken from different hospitals (Table 4). A comparative study of Table 3 and Table 4 gives ILCM 93.20 % overall accuracy (Fig. 4 (a)), F1 score (harmonic mean of precision and recall) 97.23 % (Fig. 4 (b)), MCC (Matthew's correlation coefficient) 98.26 % (Fig. 4 (c)), precision 97.12 % (Fig. 4 (d)), specificity and sensitivity is 97.21 % (Fig. 4 (e)) and 97.23 % (Fig. 4 (f)), respectively (Based on 10 % of the data, which is not involved in the training). In Golden standard (demographic) CXR all the metrics is in decreasing trend as the dataset is taken from different geographic location i.e. 83.32 % (Fig. 5 (a)) overall accuracy, F1 score 82.24 % (Fig. 5 (b)), MCC 85.28 % (Fig. 5 (c)), precision 83.57 % (Fig. 5 (d)), specificity and sensitivity is 84.45 % (Fig. 5 (e)) and 86.56 % (Fig. 5 (f)), respectively.

Precision signifies the true positives within the total number of positive predictions, whereas recall signifies true positives within the total number of positive cases in the dataset. The F1 score reflects false positives and false negatives, ranging from 0 to 1, with 1 indicating the best possible score. A good F1 score reflects a balanced trade-off between precision and recall and accurately identifies positive and negative cases. Similarly, MCC which is also a statistical metric, represent the quality of predictions made by a binary classification model. A good MCC score represents the strong complete performance of the model regarding both sensitivity and specificity.

In machine learning, strong sensitivity and specificity indicate a well-performing model that accurately distinguishes between positive examples and avoids false positives. Typically, a high sensitivity means that the model correctly identifies a significant portion of the positive examples, while a high specificity indicates that the model avoids misclassifying negative examples as positive. It is evident from Table 3 and Table 4, that the performance of ILCM is better in terms of F1 score, MCC, sensitivity, specificity precision and recall.

Furthermore, the performance of the proposed model is evaluated by analyzing the computational time (Time taken to predict the disease). The computational time for the individual models is given in Table 5. All the models perform better in the identification and localization of TB, as they take less time as compared to the ILCM. The higher computational time of the proposed model is due to its cascaded behaviour. As ILCM uses three different AI engines and each layer waits for the output from the previous layer (the experiment is done on the system having 16 GB, RAM, 2 TB SSD with i7 12th generation).

Table 5
Time Taken to Classify and Localize Disease.

Model/ Disease	Classification Time (Second)	Localization Time (Second)
AlexNet	3.289	15.858
GoogLeNet	4.025	15.836
VGGNet-16	4.032	16.853
ResNet-50	5.621	14.872
Inception V3	4.745	13.746
Xception	5.424	14.462
InceptionResNet V2	4.526	16.524
Mobile NET	3.874	18.672
DenseNet 169	4.236	19.531
NasNetLarge	3.256	15.652
DenseNet 121	5.832	16.542
ILCM (Proposed)	6.932	22.473

A comparative study between different pre-trained models and ILCM on demographic data set demonstrated that ILCM performed better as compared to different pre-trained models. The performance of the proposed model (ILCM) is better due to its incremental behaviour, as the ILCM algorithm introduces cascaded learning, which allows immediate annotation for the CXR which leads to the better accuracy of the training dataset. As the accuracy of the training dataset increases, testing accuracy starts improving. It is noted that data accuracy played an important

role to enhance the testing accuracy, which must be maintained in the training dataset.

The proposed model has "incremental behaviour", which means that the model can continue to learn and improve over time as new data becomes available. Contrarily the other models that are static and cannot be updated once they are trained. In the context of machine learning, "cascaded learning" refers to an approach where a model is trained in stages or layers, with each layer built on the output of the previous layer. In this way, the model learns more complex representations of the data as it progresses through the layers. The performance of a proposed model is better due to its incremental behaviour and cascaded learning, which shows that the model can continuously learn and improve as new data becomes available. The cascaded learning approach allows the model to learn more complex representations of the data over time. The present study clearly demonstrates that the proposed model outperforms with respect to existing state-of-the-art models, which are static.

9. Conclusion and future work

In the present study, an incremental learning-based intelligent system to detect and localize the infection caused by TB has been proposed. This model uses a multi-layered approach to diagnose the infection and recursively learn the behavior and impacts of the TB variants of the new kind. Experimental outcome demonstrates that, the ILCM model performs better on both local population data (10 % data not involved in training) as well as on the demographic dataset (Golden standard prepared from different geographic locations). In addition to this, due to its incremental approach, it also reduces the human intervention for preparing the training dataset regularly. In future, the performance of the present model can be enhance by embedding the pre-trained models.

CRediT authorship contribution statement

Satvik Vats: Conceptualization, Methodology, Investigation, Writing – original draft. **Vikrant Sharma:** Writing – original draft, Supervision, Formal analysis. **Karan Singh:** Software, Visualization, Writing – review & editing. **Anvesha Katti:** Writing – review & editing, Validation. **Mazeyanti Mohd Ariffin:** Writing – review & editing, Validation, Supervision. **Mohammad Nazir Ahmad:** Writing – review & editing, Validation. **Ali Ahmadian:** Conceptualization, Writing – review & editing, Validation, Supervision. **Soheil Salahshour:** Writing – review & editing, Validation, Supervision.

Declaration of Competing Interest

The authors declare that they have no known competing financial interests or personal relationships that could have appeared to influence the work reported in this paper.

Data availability

No data was used for the research described in the article.

References

Aboutalebi, H., Pavlova, M., Shafiee, M. J., Sabri, A., Alaref, A., & Wong, A. (2021). COVID-Net CXR-S: Deep Convolutional Neural Network for Severity Assessment of COVID-19 Cases from Chest X-ray Images. Diagnostics 2022, Vol. 12, Page 25, 12(1), 25. 10.3390/DIAGNOSTICS12010025.

Adimoolam, M., Govindharaju, K., John, A., Mohan, S., Ahmadian, A., & Ciano, T. (2022). A hybrid learning approach for the stage-wise classification and prediction of COVID-19 X-ray images. *Expert Systems, 39*(4), e12884.

Afshar, P., Heidarian, S., Naderkhani, F., Oikonomou, A., Plataniotis, K. N., & Mohammadi, A. (2020). COVID-CAPS: A capsule network-based framework for identification of COVID-19 cases from X-ray images. *Pattern Recognition Letters, 138*, 638–643. https://doi.org/10.1016/J.PATREC.2020.09.010

Albahli, S. (2020). A Deep Neural Network to Distinguish COVID-19 from other Chest Diseases Using X-ray Images. *Current Medical Imaging Formerly Current Medical Imaging Reviews), 17*(1), 109–119. https://doi.org/10.2174/1573405616666200604163954

Apostolopoulos, I. D., & Mpesiana, T. A. (2020). Covid-19: Automatic detection from X-ray images utilizing transfer learning with convolutional neural networks. *Physical and Engineering Sciences in Medicine, 43*(2), 635–640. https://doi.org/10.1007/S13246-020-00865-4/TABLES/6

Chowdhury, M. E. H., Rahman, T., Khandakar, A., Mazhar, R., Kadir, M. A., Mahbub, Z. B., … Islam, M. T. (2020). Can AI Help in Screening Viral and COVID-19 Pneumonia? *IEEE Access, 8*, 132665–132676. https://doi.org/10.1109/ACCESS.2020.3010287

Civit-Masot, J., Luna-Perejón, F., Morales, M. D., & Civit, A. (2020). Deep Learning System for COVID-19 Diagnosis Aid Using X-ray Pulmonary Images. Applied Sciences 2020, Vol. 10, Page 4640, 10(13), 4640. 10.3390/APP10134640.

Dansana, D., Kumar, R., Bhattacharjee, A., Hemanth, D. J., Gupta, D., Khanna, A., & Castillo, O. (2023). Early diagnosis of COVID-19-affected patients based on X-ray and computed tomography images using deep learning algorithm. *Soft Computing, 27*(5), 2635–2643. https://doi.org/10.1007/S00500-020-05275-Y/TABLES/8

Dinesh Jackson Samuel, R., & Rajesh Kanna, B. (2019). Tuberculosis (TB) detection system using deep neural networks. Neural Computing and Applications, 31(5), 1533–1545. 10.1007/S00521-018-3564-4/METRICS.

El Asnaoui, K., & Chawki, Y. (2020). Using X-ray images and deep learning for automated detection of coronavirus disease. 10.1080/07391102.2020.1767212, 1–12. 10.1080/07391102.2020.1767212.

Farooq, M., & Hafeez, A. (2020). COVID-ResNet: A Deep Learning Framework for Screening of COVID19 from Radiographs. https://arxiv.org/abs/2003.14395v1.

Fouladi, S., Ebadi, M. J., Safaei, A. A., Bajuri, M. Y., & Ahmadian, A. (2021). Efficient deep neural networks for classification of COVID-19 based on CT images: Virtualization via software defined radio. *Computer Communications, 176*, 234–248. https://doi.org/10.1016/J.COMCOM.2021.06.011

Hemdan, E. E.-D., Shouman, M. A., & Karar, M. E. (2020). COVIDX-Net: A Framework of Deep Learning Classifiers to Diagnose COVID-19 in X-Ray Images. https://arxiv.org/abs/2003.11055v1.

Henderson, J., & Santosh, K. (2023). Analyzing Chest X-Ray to Detect the Evidence of Lung Abnormality Due to Infectious Disease. Communications in Computer and Information Science, 1704 CCIS, 59–77. 10.1007/978-3-031-23599-3_6/COVER.

Hussain, E., Hasan, M., Rahman, M. A., Lee, I., Tamanna, T., & Parvez, M. Z. (2021). CoroDet: A deep learning based classification for COVID-19 detection using chest X-ray images. *Chaos, Solitons & Fractals, 142*, Article 110495. https://doi.org/10.1016/J.CHAOS.2020.110495

Ismael, A. M., & Şengür, A. (2021). Deep learning approaches for COVID-19 detection based on chest X-ray images. *Expert Systems with Applications, 164*, Article 114054. https://doi.org/10.1016/J.ESWA.2020.114054

Jacobi, A., Chung, M., Bernheim, A., & Eber, C. (2020). Portable chest X-ray in coronavirus disease-19 (COVID-19): A pictorial review. *Clinical Imaging, 64*, 35–42. https://doi.org/10.1016/J.CLINIMAG.2020.04.001

Jaeger, S., Candemir, S., Antani, S., Wáng, Y.-X.-J., Lu, P.-X., & Thoma, G. (2014). Two public chest X-ray datasets for computer-aided screening of pulmonary diseases. *Quantitative Imaging in Medicine and Surgery, 4*(6), 475. https://doi.org/10.3978/J.ISSN.2223-4292.2014.11.20

Jaeger, S., Karargyris, A., Candemir, S., Folio, L., Siegelman, J., Callaghan, F., … McDonald, C. J. (2014). Automatic tuberculosis screening using chest radiographs. *IEEE Transactions on Medical Imaging, 33*(2), 233–245. https://doi.org/10.1109/TMI.2013.2284099

Kc, K., Yin, Z., Wu, M., & Wu, Z. (2021). Evaluation of deep learning-based approaches for COVID-19 classification based on chest X-ray images. *Signal, Image and Video Processing, 15*(5), 959–966. https://doi.org/10.1007/S11760-020-01820-2/FIGURES/6

Khan, A. I., Shah, J. L., & Bhat, M. M. (2020). CoroNet: A deep neural network for detection and diagnosis of COVID-19 from chest x-ray images. *Computer Methods and Programs in Biomedicine, 196*, Article 105581. https://doi.org/10.1016/J.CMPB.2020.105581

Kumar Sethy, P., Kumari Behera, S., Kumar Ratha, P., & Biswas, P. (2020). Detection of coronavirus Disease (COVID-19) based on Deep Features and Support Vector Machine. www.preprints.org.

Maghdid, H., Asaad, A. T., Ghafoor, K. Z. G., Sadiq, A. S., Mirjalili, S., & Khan, M. K. K. (2021). Diagnosing COVID-19 pneumonia from x-ray and CT images using deep learning and transfer learning algorithms. 10.1117/12.2588672, 11734, 99–110. 10.1117/12.2588672.

Mahbod, A., Schaefer, G., Wang, C., Ecker, R., & Ellinge, I. (2019). Skin Lesion Classification Using Hybrid Deep Neural Networks. ICASSP, IEEE International Conference on Acoustics, Speech and Signal Processing - Proceedings, 2019-May, 1229–1233. 10.1109/ICASSP.2019.8683352.

Mahbub, M. K., Biswas, M., Gaur, L., Alenezi, F., & Santosh, K. C. (2022). Deep features to detect pulmonary abnormalities in chest X-rays due to infectious diseaseX: Covid-19, pneumonia, and tuberculosis. *Information Sciences, 592*, 389–401. https://doi.org/10.1016/J.INS.2022.01.062

Mahbub, M. K., Hossain Zamil, M. Z., Mozid Miah, M. A., Ghose, P., Biswas, M., & Santosh, K. C. (2022). MobApp4InfectiousDisease: Classify COVID-19, Pneumonia, and Tuberculosis. Proceedings - IEEE Symposium on Computer-Based Medical Systems, 2022-July, 119–124. 10.1109/CBMS55023.2022.00028.

Minaee, S., Kafieh, R., Sonka, M., Yazdani, S., & Jamalipour Soufi, G. (2020). Deep-COVID: Predicting COVID-19 from chest X-ray images using deep transfer learning. *Medical Image Analysis, 65*, Article 101794. https://doi.org/10.1016/J.MEDIA.2020.101794

Mukherjee, H., Ghosh, S., Dhar, A., Obaidullah, S. M., Santosh, K. C., & Roy, K. (2021). Deep neural network to detect COVID-19: One architecture for both CT Scans and

Chest X-rays. *Applied Intelligence, 51*(5), 2777–2789. https://doi.org/10.1007/S10489-020-01943-6/FIGURES/7
Narin, A., Kaya, C., & Pamuk, Z. (2020). Automatic Detection of Coronavirus Disease (COVID-19) Using X-ray Images and Deep Convolutional Neural Networks. Pattern Analysis and Applications 2021 24:3, 24(3), 1207–1220. 10.1007/s10044-021-00984-y.
Ozturk, T., Talo, M., Yildirim, E. A., Baloglu, U. B., Yildirim, O., & Rajendra Acharya, U. (2020). Automated detection of COVID-19 cases using deep neural networks with X-ray images. *Computers in Biology and Medicine, 121*, Article 103792. https://doi.org/10.1016/J.COMPBIOMED.2020.103792
Pande, T., Cohen, C., Pai, M., & Ahmad Khan, F. (2016). Computer-aided detection of pulmonary tuberculosis on digital chest radiographs: A systematic review. *International Journal of Tuberculosis and Lung Disease, 20*(9). https://doi.org/10.5588/IJTLD.15.0926
Punn, N. S., & Agarwal, S. (2021). Automated diagnosis of COVID-19 with limited posteroanterior chest X-ray images using fine-tuned deep neural networks. *Applied Intelligence, 51*(5), 2689–2702. https://doi.org/10.1007/S10489-020-01900-3/FIGURES/8
Rahman, T., Khandakar, A., Kadir, M. A., Islam, K. R., Islam, K. F., Mazhar, R., … Chowdhury, M. E. H. (2020). Reliable Tuberculosis Detection using Chest X-ray with Deep Learning, Segmentation and Visualization. *IEEE Access, 8*, 191586–191601. https://doi.org/10.1109/ACCESS.2020.3031384
Roy, S., & Santosh, K. C. (2023). Analyzing Overlaid Foreign Objects in Chest X-rays—Clinical Significance and Artificial Intelligence Tools. Healthcare 2023, Vol. 11, Page 308, 11(3), 308. 10.3390/HEALTHCARE11030308.
Santosh, K., Allu, S., Rajaraman, S., & Antani, S. (2022). Advances in Deep Learning for Tuberculosis Screening using Chest X-rays: The Last 5 Years Review. *Journal of Medical Systems, 46*(11), 1–19. https://doi.org/10.1007/S10916-022-01870-8/TABLES/7
Santosh, K. C. (2020). AI-Driven Tools for Coronavirus Outbreak: Need of Active Learning and Cross-Population Train/Test Models on Multitudinal/Multimodal Data. *Journal of Medical Systems, 44*(5), 1–5. https://doi.org/10.1007/S10916-020-01562-1/FIGURES/5
Santosh, K. C. (2020). COVID-19 Prediction Models and Unexploited Data. *Journal of Medical Systems, 44*(9), 1–4. https://doi.org/10.1007/S10916-020-01645-Z/METRICS
Santosh, K. C., & Antani, S. (2018). Automated Chest X-Ray Screening: Can Lung Region Symmetry Help Detect Pulmonary Abnormalities? *IEEE Transactions on Medical Imaging, 37*(5), 1168–1177. https://doi.org/10.1109/TMI.2017.2775636
Santosh, K. C., Ghosh, S., & Ghoshroy, D. (2022). Deep Learning for Covid-19 Screening Using Chest X-Rays in 2020: A Systematic. *Review, 36*(5). https://doi.org/10.1142/S0218001422520103
Santosh, K. C., Vajda, S., Antani, S., & Thoma, G. R. (2016). Edge map analysis in chest X-rays for automatic pulmonary abnormality screening. *International Journal of Computer Assisted Radiology and Surgery, 11*(9), 1637–1646. https://doi.org/10.1007/S11548-016-1359-6/METRICS
Santosh, K., & Ghosh, S. (2021). Covid-19 Imaging Tools: How Big Data is Big? *Journal of Medical Systems, 45*(7), 1–8. https://doi.org/10.1007/S10916-021-01747-2/TABLES/2
Sitaula, C., & Hossain, M. B. (2021). Attention-based VGG-16 model for COVID-19 chest X-ray image classification. *Applied Intelligence, 51*(5), 2850–2863. https://doi.org/10.1007/S10489-020-02055-X/TABLES/11
Tabik, S., Gomez-Rios, A., Martin-Rodriguez, J. L., Sevillano-Garcia, I., Rey-Area, M., Charte, D., … Herrera, F. (2020). COVIDGR Dataset and COVID-SDNet Methodology for Predicting COVID-19 Based on Chest X-Ray Images. *IEEE Journal of Biomedical and Health Informatics, 24*(12), 3595–3605. https://doi.org/10.1109/JBHI.2020.3037127
Taresh, M. M., Zhu, N., Ali, T. A. A., Hameed, A. S., & Mutar, M. L. (2021). Transfer Learning to Detect COVID-19 Automatically from X-Ray Images Using Convolutional Neural Networks. *International Journal of Biomedical Imaging, 2021*. https://doi.org/10.1155/2021/8828404
Vaishya, R., Javaid, M., Khan, I. H., & Haleem, A. (2020). Artificial Intelligence (AI) applications for COVID-19 pandemic. *Diabetes & Metabolic Syndrome: Clinical Research & Reviews, 14*(4), 337–339. https://doi.org/10.1016/J.DSX.2020.04.012
Zaidi, S. Z. Y., Akram, M. U., Jameel, A., & Alghamdi, N. S. (2022). A deep learning approach for the classification of TB from NIH CXR dataset. *IET Image Processing, 16*(3), 787–796. https://doi.org/10.1049/IPR2.12385

Dr Satvik Vats is an Assistant Professor in the Dept. of Computer Science and Engineering, Graphic Era Hill University, Dehradun. He is done his PhD in Computer Science and Engineering from Birla Institute of Technology, Mesra-Ranchi (Deemed University), Jharkhand, India. He has published several research papers in refereed journals/Conferences of International repute (SCI/SCIE/ESCI/SCOPUS/WEB of SCIENCE) with 13 Patents and three books. He has published two book chapters in the books of international publishers. He is awarded the "Young Scholar Award" at the International Conference on Network and Cryptology 2020, organized by the School of Computer and Systems Sciences, Jawahar Lal Nehru University (JNU), New Delhi. Currently, he is working on a "Hybrid Approach of Machine learning Techniques such as recommender systems and supervised and unsupervised learning with integration of Big Data analytics and deep learning concepts.

Dr. Vikrant Sharma is an Assistant Professor in the Department of Computer Science and Engineering at Graphic Era Hill University, Dehradun, Uttarakhand, India. He received a Diploma (Information Technology) from Government Polytechnic College, Hamirpur, Himachal Pradesh, India in 2007, BTech. Degree (IT) from the Himachal Pradesh University (HPU), Shimla, India in 2010, M Tech (Computer Science and Engineering) from M.M. University, Mullana, Haryana, India in 2013. He received PhD. in Computer Science and Engineering from the Department of Computer Science and Engineering, Uttarakhand Technical University in 2018. The author has published several papers in International Journals and Conferences. He is working in the field of Security and Fault Tolerance and deployment in a mobile ad-hoc network, Wireless Sensor Networks, Internet of Things, and Machine Learning.

Dr. Karan Singh (SMIEEE) is working with the School of Computer & Systems Sciences, Jawaharlal Nehru University, New Delhi. He is a reviewer of IEEE & Elsevier conferences and a reviewer of International Journals & IEEE Transactions. He is an Editorial Board Member of the Journal of Communications and Network (CN), USA. He published more than a hundred plus research papers in the journal SCI/SCIE/Scopus and good conferences. He organized various workshops, Sessions, conferences, and training. Dr. Singh worked as General Chair of the International Conference (Qshine) in the year 2013 at Gautam Buddha University. He organized as Chair of the International Conference "NetCrypt 2020" at JNU, New Delhi. He was nominated for Who's who in World in the year 2008. Dr. Singh has joined a Professional member Association for Computing Machinery (ACM), New York, Computer Science Teachers Association (CSTA) the U.S.A, Computer Society of India(CSI), Secunderabad, India, Cryptology Research Society of India (CRSI), Kolkata, India, Institute of Electrical and Electronics Engineers (IEEE), USA, International Association of Computer Science and Information Technology (IACSIT), Singapore, Institute for Computer Sciences, Social-Informatics and Telecommunications Engineering (ICST), America, International Association of Engineers (IAENG), Hong Kong, Association of Computer Electronics and Electrical Engineers (ACEEE), India, Internet Society(ISOC), USA and Academy & Industry Research Collaboration Center (AIRCC), India.